High-Power Tunable FDD Front-End Employing a Balanced CMOS N-Path Receiver and Evanescent-Mode Cavity Filters

Nimrod Ginzberg[1], Thomas R. Jones[2], Avi Lax[1], Erez Zolkov[1], Michael D. Sinanis[2], Dimitrios Peroulis[2], Emanuel Cohen[1]
[1]Faculty of Electrical and Computer Engineering, Technion, Haifa, Israel
[2]Elmore Family School of Electrical and Computer Engineering, Purdue University, IN, USA

***Abstract*— A single-antenna, frequency-tunable FDD front-end supporting simultaneous transmit (TX) and receive (RX) operation with high power handling capabilities and low TX and RX losses is presented. The system comprises a balanced CMOS N-path receiver in series with tunable evanescent-mode filters, and leverages frequency-selective reflectivity and matching for quadrature signal construction and self-interference cancellation at corresponding ports of interest. A measured 65 nm CMOS receiver prototype with manufactured cavity filters demonstrated 38 dBm blocker tolerance (B1dB) around 1 GHz at 100 MHz TX−RX spacing with no RX EVM degradation, < 0.4 dB TX insertion loss, and 3.5−4.5 dB RX NF over 0.9−1.8 GHz tunable frequency range.**

***Keywords*— Evanescent-mode cavity filter, frequency-division duplex (FDD), interference cancellation, N-path mixer.**

I. Introduction

Modern wireless communications standards, such as the 5G new radio (NR), define significantly denser multi-band operation relative to 4G, requiring advanced frequency-division duplexing (FDD) systems for flexible and agile spectrum utilization. However, incorporating frequency tunability into the FDD front-end is typically associated with increased insertion losses (IL) and poorer TX−RX isolation. Self-interference cancellation (SIC) approaches that enhance initially relaxed TX−RX coupling scenarios have been reported [1], and in [2], [3], tunable diplexers with SIC were proposed. In all these techniques, cancellation bandwidth, IL, noise figure (NF), and antenna VSWR coverage remain major challenges.

Many of the above challenges may be circumvented by incorporating digital cancellation approaches. In [4], a diversity receiver assisted by an auxiliary noise-canceling (NC) path with baseband processing was proposed, and in [5], a balanced receiver providing high integration and low loss for a single-antenna interface with digital baseband interference cancellation was introduced. However, both [4] and [5] exhibit limited power handling and linearity performance.

This paper presents a single-antenna, frequency-agile FDD front-end comprising a combination of tunable evanescent-mode filters and an integrated, balanced CMOS N-path receiver assisted by a digital interference cancellation algorithm. Incorporating high-Q and high-power tunable filters in the RX path unlocks high power handling capabilities of a CMOS-based receiver for applications that are less sensitive to the radio head's size, such as cellular base stations.

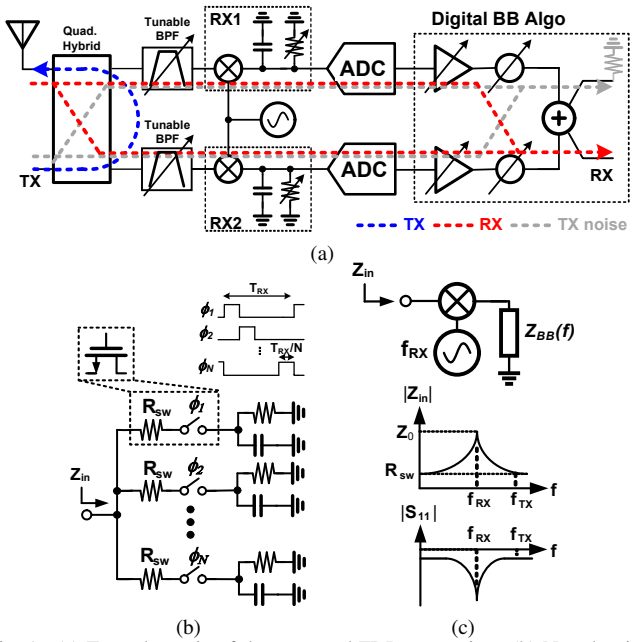

Fig. 1. (a) Top schematic of the proposed FDD transceiver, (b) N-path mixer schematic with its clock timing diagrams, (c) behavioral plots of the N-path input impedance and return loss.

II. System Architecture and Operating Principle

The proposed receiver front-end is shown in Fig. 1a. It consists of two CMOS N-path receivers, as in Fig. 1b, interfacing a quadrature hybrid via frequency-selective and tunable evanescent-mode filters. The TX port and the antenna are connected to the hybrid's other two ports. We leverage the frequency-selectivity of the N-path mixers' input impedance (see Fig. 1c) to create initial TX-RX isolation, which is enhanced by the tunable evanescent-mode filters that also increase the system's power handling capabilities.

A. TX Band

The TX band can be selected anywhere on the spectrum in the stop-band of the tunable filters, in which they present high input impedance. This stop-band impedance is further enhanced by the cascade of the filters with the low out-of-band (OOB) input impedance of the N-path mixers, as will be shown in Section III, creating a strong impedance mismatch and high reflectivity. TX signals departing from the quadrature hybrid's TX port reflect at the filters interface and reconstruct in-phase at the antenna with minimal insertion loss.

B. RX Band

In the RX band, the mixers are designed to show input impedance matched to the antenna impedance, while the bandpass filters' pass-band is tuned to the RX band. As a result, RX signals entering the system from the antenna are absorbed in the matched receivers and reconstructed in quadrature in the digital baseband. TX noise in the RX band is also absorbed in the receivers and cancelled out in the digital baseband by the same quadrature mechanism regardless of the antenna VSWR. Consequently, antenna VSWR impact on RX NF is minor, even for high antenna reflection and realistic N-path return loss.

III. Analysis of the Evanescent-Mode Filter and N-Path Mixer Interaction

The main target in employing cavity filters with CMOS N-path mixers is to achieve OOB linearity better than 30 dBm at around 100 MHz offset from the RX frequency for 20 MHz signals. The N-path was designed to tolerate up to 10 dBm OOB TX blocker, and together with the cavity filter's rejection at 100 MHz offset of at least 20 dB, the design target can be met.

The cascade of the cavity filter and the N-path OOB impedance yields a combined filtering response. To evaluate the effect of the N-path loading on the cavity filter compared to a Z_0 load, we write the power delivered by the filter, having an output impedance $Z_{filter,out}$, to a load Z_L:

$$P_{\text{out}} = \frac{\left(V_{\text{out}} \frac{Z_L}{Z_L + Z_{filter,out}}\right)^2}{2Z_L} \tag{1}$$

where V_{out} is the voltage across Z_L. The power difference between an N-path load of $Z_L = R_{SW}$ and a Z_L = 50 Ω load can be calculated by substituting each of these impedances in (1) and taking the ratio:

$$\Delta P_{\text{out}} = \frac{R_{SW}}{50} \left(\frac{Z_{\text{filter,out}} + 50}{Z_{\text{filter,out}} + R_{SW}} \right) \tag{2}$$

For $R_{SW}, 50\ \Omega \ll Z_{\text{filter,out}}$, we get $\Delta P_{\text{out}} \approx R_{SW}/50$. The N-path standalone OOB rejection in a system with a characteristic impedance of Z_0 is given by:

$$S_{21,\text{Npath}} = 2\sqrt{\frac{Z_0}{R_{SW}}} \frac{R_{SW}}{R_{SW} + Z_0} \tag{3}$$

Substituting Z_0 = 50 Ω and assuming $R_{SW} \ll Z_0$, equation (3) reduces to $S_{21,Npath} \approx 2\sqrt{R_{SW}/50}$. Therefore, the improvement in the cavity filter's OOB rejection when interfacing an N-path impedance of R_{SW} = 4 Ω (as of the N-path in our system) instead of 50 Ω is:

$$\Delta OOB = dB_{20}(S_{21,\text{Npath}}) - dB_{10}(\Delta P_{\text{out}}) \approx 6\ dB \tag{4}$$

The cavity filter was designed to show high impedance between 1−2 GHz, and specifically very high impedance just besides the pass-band, as shown in Fig. 2(a). The improvement in OOB rejection due to the low N-path impedance in series versus R_{SW} and frequency is shown in Fig. 2(b)-(c). These figures consider a more realistic calculation based on the actual filter and N-path S-parameters measurements, showing a 5.3 dB improvement at a 100 MHz offset.

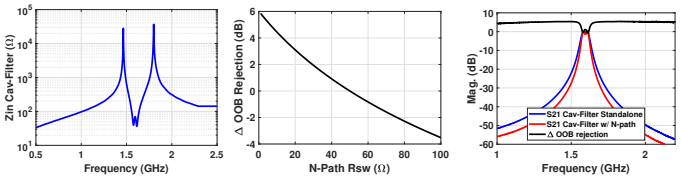

(a) (b) (c)

Fig. 2. (a) Measured cavity filter input impedance, (b) cavity filter OOB rejection improvement versus R_{SW} and (c) frequency.

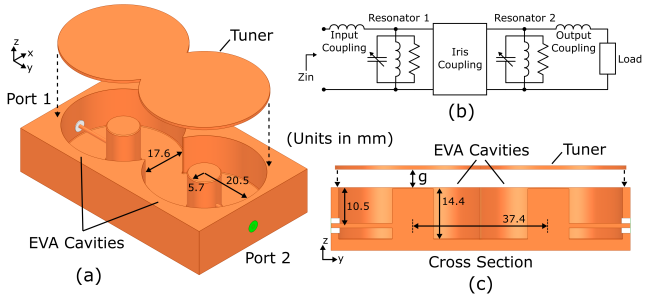

Fig. 3. (a) 3D layout of the two-pole evanescent-mode tunable filter, (b) equivalent circuit, and (c) cross-section.

IV. Tunable Bandpass Filter Implementation

To simultaneously meet the design requirements for low in-band insertion loss, high OOB rejection, wide harmonic suppression, high power handling, and octave tuning range, high-Q two-pole bandpass filters (BPF) were designed and manufactured using evanescent-mode resonators [6], [7], [8].

Fig. 3 shows the 3D layout and equivalent circuit of the two-pole evanescent-mode BPF design. A capacitive post loads a high-Q cylindrical waveguide cavity, lowering the resonance frequency of the fundamental TM_{010} mode with minimal impact on the second-order TM_{110} mode, providing both miniaturization and wide spurious-free bandwidth [9].

A flexible metalized membrane above the post provides a wide tuning range by adjusting the gap g. New Scale Technologies M3-LS microactuators are used for the present embodiment to adjust the membrane's height, with high resolution of 0.5 μm [10]. An inductive iris is formed between two evanescent resonators, providing inter-resonator coupling for a two-pole BPF response. External input/output coupling is provided by the flanged SMA pin extending through the cavity's side and touching the post.

V. Digital TX Noise Cancellation in the RX Band

The algorithm for TX noise cancellation in the RX band uses measurements of the in-phase and in-quadrature TX-to-RX transfer functions (TF) and calculates their inverse. Since transfer function calculation is only valid in LTI systems, we inject the reference TX signal, $x_{ref}^{TX}(t)$, with low input power to ensure linearity and set its center frequency,

f_c, similar to the RX center frequency. The time-domain IQ outputs, $y^I_{norm}(t)$ and $y^Q_{norm}(t)$, are normalized and time-aligned. After performing FFT, the inverse TFs are:

$$\left(\frac{Y^I_{norm}(f)}{X^{TX}_{ref}(f)}\right)^{-1} \quad ; \quad \left(\frac{Y^Q_{norm}(f)}{X^{TX}_{ref}(f)}\right)^{-1} \tag{5}$$

These TFs are then used to cancel the TX noise in the RX band during simultaneous transmission and reception in FDD mode. The combined signals, comprising the desired RX signal and the TX noise signal, denoted by $Y^{I^{norm}}_{joint}(f)$ and $Y^{Q^{norm}}_{joint}(f)$, are multiplied by the corresponding inverse TF. Then, RX signal reconstruction and TX noise cancellation are achieved by the following subtraction:

$$Y^{I^{norm}}_{\text{Joint}}(t)\cdot\left(\frac{Y^I_{norm}(f)}{X^{TX}_{ref}(f)}\right)^{-1} - Y^{Q^{norm}}_{\text{Joint}}(t)\cdot\left(\frac{Y^Q_{norm}(f)}{X^{TX}_{ref}(f)}\right)^{-1} \tag{6}$$

Next, we implement an equalizer based on peak correlation and channel impulse response for accurate RX demodulation.

VI. Measurements

The measurement setup is shown in Fig. 4. It consists of a 65 nm CMOS chip comprising two N-path mixers [11]. The chip is attached and wire-bonded to an FR4 PCB and connected through the tunable filters to an Anaren 1H0565 quadrature hybrid. The TX path employs a Qorvo QPD1004 GaN PA and a Mini-Circuits PHA-202+ driver. An Agilent N5182B Signal Generator and a Keysight M8190 AWG were used to transmit 16-QAM, 10 MHz TX and RX signals into the systems, respectively. The LO signal to the N-path mixers was injected using another Agilent N5182B Signal Generator. The output TX signal at the antenna port was coupled through a 10 dB directional coupler and recorded using a Keysight N9040B Spectrum Analyzer, and the baseband IQ RX data was sampled by a Keysight DSOS604A Oscilloscope. A Keysight P9374A Network Analyzer was used for S-parameters measurements. The filters' actuators and the CMOS chip configurations were controlled by a computer.

A. Standalone Tunable Evanescent-Mode Filter

A picture of the manufactured filter is shown in Fig. 4(c). Fig. 5(a) plots the simulated and measured scattering parameters with excellent agreement. The filter achieves a tuning range from 0.8 to 1.8 GHz (2.35:1), with corresponding gaps g from 192 to 670 μm, respectively. The in-band insertion loss is below 0.41 dB across the entire tuning range, and below 0.3 dB when tuned between 1 to 1.6 GHz. The OOB rejection is greater than 22 dB at $\pm$100 MHz from f_c across the tuning range, and greater than 26 dB at tuning ranges below 1.3 GHz. Fig. 5(b) shows a large spurious-free range up to approximately 8.2 GHz. Power handling beyond 100 W of an equivalent evanescent-mode filter has already been demonstrated [6].

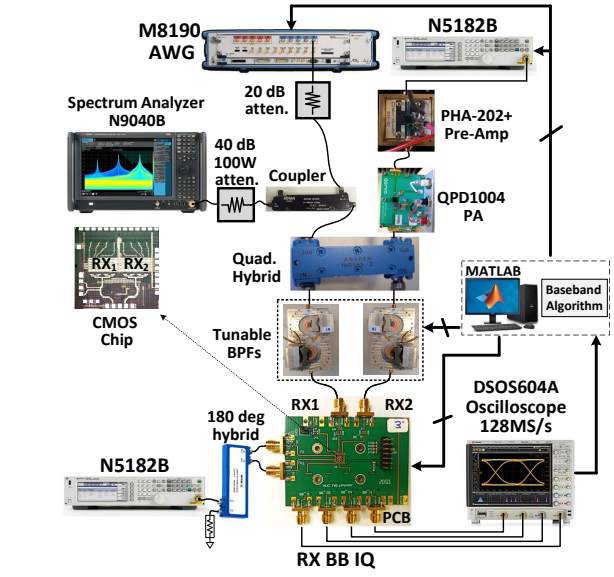

(a)

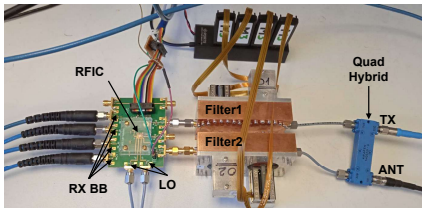

(b)

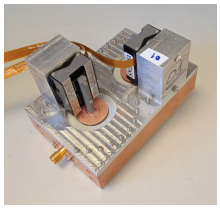

(c)

Fig. 4. Setup (a) schematic and (b) photo. (c) Tunable filter photo.

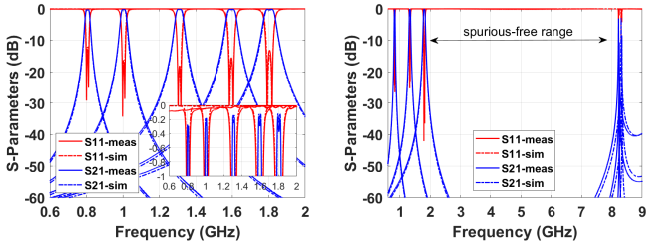

(a) (b)

Fig. 5. (a) Measured and simulated scattering parameters ($|S_{11}|$ and $|S_{21}|$) of the tunable cavity filter across its tuning range. (b) Spurious-free range.

B. Combined N-path and Cavity Filter Response

The combined small-signal response of the N-path with the cavity filter is shown in Fig. 6(a). TX IL $<$ 0.4 dB and input matching $>$ 12 dB were measured across the tuning range.

Fig. 6(b) shows RX compression at 1 GHz versus TX output power (B1dB) at 1.1 and 1.15 GHz. When the TX was operated at 1.15 GHz, no RX compression was observed up to the PA's saturated power of 39 dBm at this frequency. For 1.1 GHz TX frequency, RX B1dB was 38 dBm, which can be attributed to 10 dBm of N-path B1dB at 100 MHz offset, 25 dB of cavity filter rejection, and 3 dB power split at the quadrature hybrid.

In the dynamic measurements, the TX signal was transmitted at 25 dBm average power around 1.1 GHz in

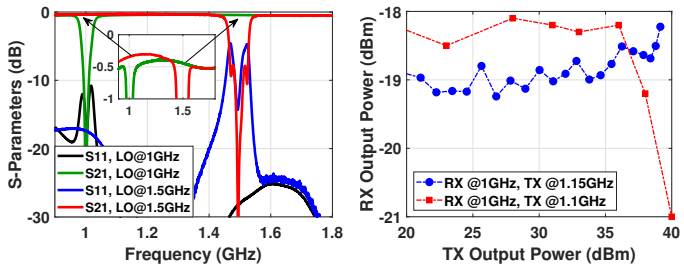

(a) (b)

Fig. 6. (a) Measured combined response of the N-path cascaded to the cavity filter. (b) Measured RX compression versus TX power.

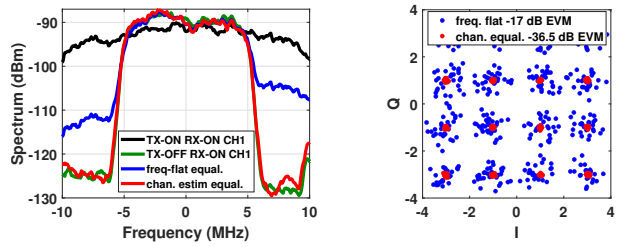

(a) (b)

Fig. 7. Measured (a) RX spectrum and (b) constellation under TX signal before and after TX noise cancellation in the RX band.

conjunction with a −40 dBm RX signal around 1 GHz, such that the TX noise level roughly equals the RX signal power. Fig. 7 shows the RX spectrum and constellation before and after the digital TX noise cancellation algorithm. Before applying any equalization, RX SNR is zero. Frequency-flat equalization achieves limited noise rejection and poor RX EVM of −17 dB, while full equalization based on channel estimation, according to Section V, suppresses the entire TX noise and fully recovers the RX signal with −36.5 dB EVM, similar to a standalone RX signal with no simultaneous TX.

NF measurements are shown in Fig. 8. The filter and the hybrid create a combined loss of roughly 0.4 dB, which is the amount of NF degradation compared to the standalone balance N-path receiver [11], meaning that the filter's harmonic impedance does not impact the N-path's NF.

Table 1 compares this work with the state-of-the-art, showing that an N-path receiver preceded by tunable evanescent-mode filters can achieve the highest power handling and B1dB along with the lowest TX IL and competitive RX NF.

VII. Conclusion

A 0.9-1.8 GHz tunable FDD transceiver front-end comprising evanescent-mode filters and a balanced 65 nm CMOS N-path receiver was presented. The system supports tunability over the entire frequency range and allows FDD operation with as low as 100 MHz TX-RX separation with degradation lower than 0.4 dB for both TX and RX paths and TX average power levels higher than 25 dBm. Experimental characterization with 10 MHz, 16-QAM signals demonstrates successful RX signal demodulation and TX noise cancellation

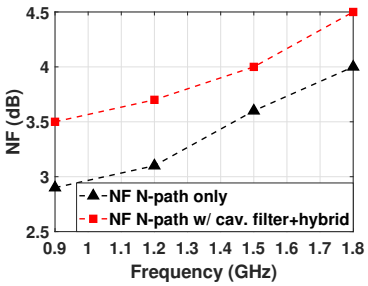

Fig. 8. NF measurements with and without the cavity filter.

Table 1. Comparison Table

	This work	[3]	[2]	[5]
Architecture	**Balanced N-Path RX+EMF***	EMF*+SIC	Switch Cap + SIC	Balanced N-Path Mixer First RX
Freq. range	**0.9–1.8 GHz**	0.86–1.03 GHz	710–970 MHz	0.75–2 GHz
ANT–RX NF	**3.5-4.5 dB**	4 dB	5–7 dB**	2.8–5.8
TX–RX offset	**100 MHz**	50 MHz	110 MHz	>200 MHz
TX–ANT IL	**0.4 dB**	1.6–2.2 dB	4.6–8.4 dB	> 2 dB
RX B1dB	**> 38 dBm**	-	-	18 dBm
TX power at RX EVM test	**25 dBm**	10 dBm	22 dBm***	5 dBm

* Evanescent-mode filter ** no LNA *** CW

in the RX band using signal processing algorithms in digital baseband, making the proposed system a competitive candidate for single-antenna FDD base-stations applications.

References

[1] J. Zhou, T. -H. Chuang, T. Dinc and H. Krishnaswamy, "Integrated Wideband Self-Interference Cancellation in the RF Domain for FDD and Full-Duplex Wireless," in *IEEE Journal of Solid-State Circuits*, vol. 50, no. 12, pp. 3015-3031, Dec. 2015.

[2] A. Goel, B. Analui and H. Hashemi, "Tunable Duplexer With Passive Feed-Forward Cancellation to Improve the RX-TX Isolation," in *IEEE Transactions on Circuits and Systems I: Regular Papers*, vol. 62, no. 2, pp. 536-544, Feb. 2015.

[3] M. Abu Khater, J. Zhou, Y. -C. Wu, H. Krishnaswamy and D. Peroulis, "A tunable 0.86–1.03 GHz FDD wireless communication system with an evanescent-mode diplexer and a self-interference-cancelling receiver," *2017 IEEE MTT-S International Microwave Symposium (IMS)*, 2017.

[4] D. Montanari et al., "An FDD Wireless Diversity Receiver With Transmitter Leakage Cancellation in Transmit and Receive Bands," in *IEEE Journal of Solid-State Circuits*, vol. 53, no. 7, July 2018.

[5] E. Zolkov, N. Ginzberg and E. Cohen, "An Integrated Reconfigurable SAW-Less Quadrature Balanced N-Path Transceiver for Frequency-Division and Half Duplex Wireless," 2022 IEEE Radio Frequency Integrated Circuits Symposium (RFIC), 2022, pp. 255-258.

[6] M. D. Sinanis, P. Adhikari, T. R. Jones, M. Abdelfattah, and D. Peroulis, "High-Q high power tunable filters manufactured with injection molding technology," *IEEE Access*, vol. 10, pp. 19643–19653, Feb 2022.

[7] D. Peroulis, E. Naglich, M. Sinani, and M. Hickle, "Tuned to resonance: Transfer-function-adaptive filters in evanescent-mode cavity-resonator technology," *IEEE Microw. Mag.*, vol. 15, no. 5, pp. 55–69, Jul 2014.

[8] Z. Yang, D. Psychogiou and D. Peroulis, "Design and optimization of tunable silicon-integrated evanescent-mode bandpass filters," *IEEE Trans. Microw. Theory Techn.*, vol. 66, no. 4, pp. 1790-1803, Apr 2018.

[9] E. J. Naglich, J. Lee and D. Peroulis, "Tunable bandstop filter with a 17-to-1 upper passband," in *IEEE MTT-S Int. Microw. Symp. Dig.*, Montreal, QC, Canada, Jun. 2012, pp. 1-3.

[10] *New Scale Technologies M3-LS Linear Smart Stage*, Accessed: December 1, 2022. [Online]. Available: https://www.newscaletech.com/wp-content/uploads/M3-LS-datasheet.pdf

[11] E. Zolkov and E. Cohen, "A Mixer-First Receiver With Enhanced Matching Bandwidth by Using Baseband Reactance-Canceling LNA," in SSCL, vol. 4, pp. 109-112, 2021.